JOURNAL OF MATERIALS SCIENCE 26 (1991) 1045–1050

Influence of the high temperature treatment of zinc phosphate conversion coatings on the corrosion protection of steel

T. SUGAMA, L. E. KUKACKA, N. CARCIELLO, J. B. WARREN
Process Sciences Division, Department of Applied Science, Brookhaven National Laboratory, Upton, New York 11973, USA

An anhydrous α-$Zn_3(PO_4)_2$ phase converted by the dehydration of hydrous zinc phosphate, $Zn_3(PO_4)_2 \cdot 2H_2O$, crystal coatings in air at a temperature of approximately 300 °C, significantly enhances the corrosion resistance of steel, and also reduces the susceptibility of the crystals to alkaline dissolution. A subsequent $\alpha \rightarrow \gamma$ phase transition at approximately 500 °C results in a poor protection behaviour, because of the formation of numerous microcracks on the crystal faces.

1. Introduction

Earlier work at Brookhaven National Laboratory (BNL) indicated that crystalline conversion coatings deposited on steel surfaces through a dissolution–recrystallization process of the original zinc orthophosphate dihydrate [$Zn_3(PO_4)_2 \cdot 2H_2O$], not only enhance the corrosion protection of steel, but also significantly improve the adherence properties to organic topcoatings [1, 2]. The major phase in the insoluble conversion coatings, which is responsible for these improvements, was identified to be the same $Zn_3(PO_4)_2 \cdot 2H_2O$, (Zn·Ph) as that used as a convertible material.

From the viewpoint of crystal molecular structure, since Zn·Ph layers contain a certain amount of crystallized water, it should be considered that when thermal barrier organic topcoat systems such as polyimide [3], polybenzimidazoles [4], polyquinoxalines [5], and polyphenylene sulphide [6], are applied directly to the Zn·Ph surface, high-temperature treatment of the topcoats to form solid polymer films will lead to interfacial disbondment and separation brought about by the dehydration of the Zn·Ph. This failure is associated with the formation of weak boundary layers, resulting in poor corrosion protection. It is very important, therefore, to gain fundamental knowledge regarding the thermal degradation and behaviour of Zn·Ph, prior to studying the interfacial chemical nature between the high-temperature performance polymers and the crystalline Zn·Ph. As already reported by Kojima, *et al.* [7], the phase transition of hopeite, $Zn_3(PO_4)_2 \cdot 4H_2O$, with increased temperature in nitrogen gas, occurs through the following processes

$$Zn_3(PO_4)_2 \cdot 4H_2O \xrightarrow{80\,^\circ C} Zn_3(PO_4)_2 \cdot 2H_2O \xrightarrow{235\,^\circ C}$$

$$\alpha\text{-}Zn_3(PO_4)_2 \xrightarrow{965\,^\circ C} \beta\text{-}Zn_3(PO_4)_2 \xrightarrow[(Melt)]{1055\,^\circ C} \gamma\text{-}Zn_3(PO_4)_2$$

These authors also indicated that a similar phase transition was observed in hot air.

The aim of the present study was, therefore, to determine the correlation between the phase transition or conformation of the $Zn_3(PO_4)_2 \cdot 2H_2O$ phase, as a function of temperature, and to understand how the thermally transformed phases protect steel from corrosion. In order to obtain this information, Zn·Phs precipitated on steel were exposed to air at temperatures up to 500 °C. Electrochemical testing of the converted phases was then conducted to provide data on the corrosion protection. Since cathodic delamination occurring at polymer-conversion coating interfaces is due mainly to alkaline dissolution of the phosphate coating [8], the extent of dissolution was also investigated. This was accomplished after soaking the different crystal phases in a 0.1 M NaOH solution at 25 °C.

2. Experimental procedure

2.1. Materials

The metal substrate used was a high strength cold-rolled sheet steel supplied by the Bethlehem Steel Corporation. The steel contained 0.06 wt % C, 0.6 wt % Mn, 0.6 wt % Si, and 0.07 wt % P. The formulation for the zinc phosphating liquid used in this study consisted of 1.3 wt % zinc orthophospate dihydrate, 2.6 wt % H_3PO_4, and 96.1 wt % water.

The Zn·Ph conversion coatings were prepared in accordance with the following sequence. As the first step in the preparation, the steel surface was wiped with acetone-soaked tissues to remove any surface contamination due to mill oil. The steel was then immersed for up to 20 min in the conversion solution described above at a temperature of 80 °C. After immersion, the surface was rinsed with water, and then dried in an oven at 60 °C for 30 min.

0022–2461/90 $03.00 + .12

2.2. Measurements

In order to study the phase transition and conversion of Zn·Ph coatings as a function of temperature up to 500 °C in air, the Zn·Ph crystal layers deposited on the steel surfaces were removed by scraping. They were then ground to a size of 325 mesh (0.044 mm) for use in analyses performed using the combined techniques of thermogravimetric analysis (TGA) coupled with differential thermal analysis (DTA), infrared (IR) spectroscopy, and X-ray powder diffraction (XRD).

The electrochemical testing for data on corrosion was performed with an EG & C Princeton Applied Research Model 362-1 Corrosion Measurement System. The electrolyte was a 0.5 M sodium chloride solution made from distilled water and reagent grade salt. The specimen was mounted in a holder and then inserted into a EG & G Model K47 electrochemical cell. The tests were conducted in the aerated 0.5 M NaCl solution at 25 °C, and the exposed surface area of the specimens was 1.0 cm^2. The cathodic and anodic polarization curves were determined at a scan rate of 0.5 mV sec^{-1} in the corrosion potential range of − 1.2 to 0.3 V.

Alterations to the surface microtopography images and the changes in surface chemical components of the heat-treated Zn·Ph coatings before and after exposure to a 0.1 M NaOH solution for 1 hr, were explored using AMR 10 nm scanning electron microscopy (SEM) associated with TN-2000 energy-dispersion X-ray spectrometry (EDX).

3. Results and discussion

Fig. 1 shows typical TGA–DTA curves for a powdered Zn·Ph sample after drying at 60 °C for 24 h. The curve indicates that heating to 170 °C results in a weight loss of approximately 4%. Based upon the broad endothermic peak on the DTA curve at the same temperature, the weight loss is likely to be due to the removal of evaporable water such as free water and water adsorbed on the crystal. The curve also illustrates a manifestation of the kinetics of the elimination of non-evaporable water upon heating the Zn·Ph compounds. The reduction in weight of approximately 8% which occurs over the temperature range 170 to 350 °C is probably associated with the liberation of crystallized water existing in the Zn·Ph compounds, and this loss appears to be related directly to the prominent DTA endothermal peak at 345 °C. Beyond approximately 400 °C, the weight loss curve seems to level off, thereby suggesting that the conversion of the hydrous Zn·Ph compound into an anhydrous one is completed at approximately that temperature.

In addition to the TGA–DTA studies, IR and XRD analyses were also performed, and these data are shown in Figs 2 and 3, respectively. An estimate of the rate of liberation of crystallized water from the Zn·Ph compounds as a function of temperature, was made by plotting the variations in IR absorbance with temperature at a frequency of 1610 cm^{-1} which reveals the H–O–H bending vibration of water of crystallization (see Fig. 2). As is evident from the absorbance against temperature curve, the absorbance decreased rapidly upon heating to 300 °C and beyond this temperature, levelled off. This suggests that to a large extent, the dehydration of Zn·Ph occurs in air at temperatures less than 300 °C. In fact, the XRD pattern (see Fig. 3 – 300 °C) for the diffraction range 0.256 to 0.371 nm, clearly indicates the formation of anhydrous α-$Zn_3(PO_4)_2$ as the major phase and anhydrous

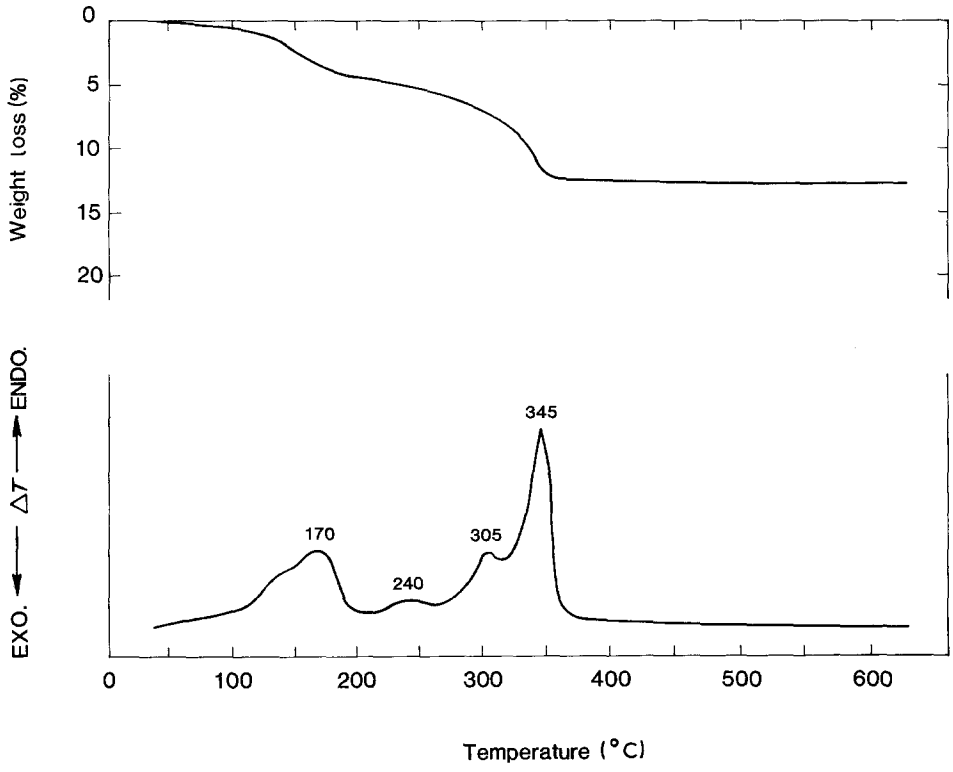

Figure 1 Typical TGA–DTA curves for zinc phosphate conversion coatings deposited on steel surfaces.

γ-$Zn_3(PO_4)_2$ as a minor phase. All of XRD lines for samples treated at temperature < 200 °C are associated with the original $Zn_3(PO_4)_2 \cdot 2H_2O$ phase. This implies that the conversion into the anhydrous phases occurs at a temperature ranging from 200 to 300 °C.

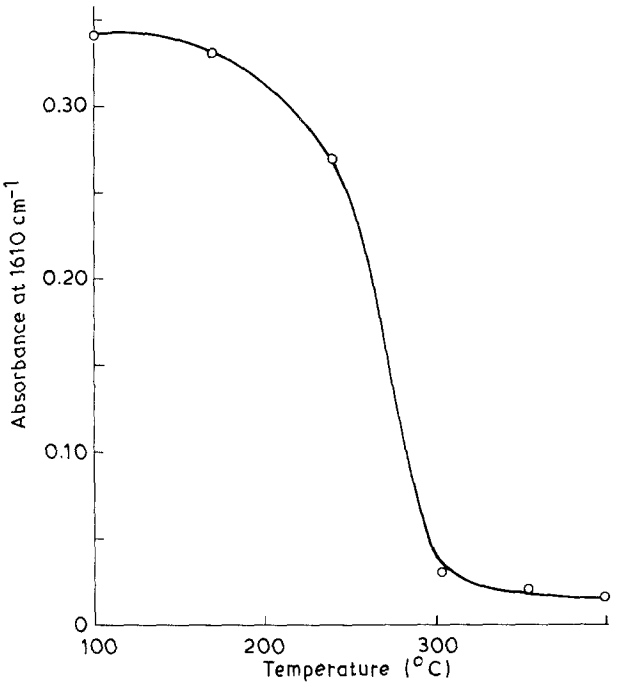

Figure 2 Changes in IR absorbance of H–O–H at 1610 cm^{-1} as a function of temperature for zinc phosphate coatings deposited on steel surfaces.

As indicated by the presence of a weak diffraction line at 0.293 nm which ascribes to the hydrous Zn·Ph compounds, the hydrous → anhydrous conversion was not, however, complete at 300 °C. This line disappeared when the sample was oven-heated at 400 °C for 1 h. At 500 °C, the tracing indicates the growth of line intensities at 0.279 and 0.343 nm, and weak peaks at 0.307, 0.315, and 0.360 nm. Since the former two intense lines represent the presence of a relatively large amount of $-Zn_3(PO_4)_2$, it appears that heat treatment at 500 °C promotes $\alpha \rightarrow \gamma$ phase transition processes. Based upon the above information, a summary of the phase transition of $Zn_3(PO_4)_2 \cdot 2H_2O$ at temperatures up to 500 °C is given in Table I. The resulting phase transitions are quite different from those obtained during an earlier study by Kojima [7] of the thermal deterioration of hopeite, $Zn_3(PO_4)_2 \cdot 4H_2O$. While the former undergoes the following conversion processes at relatively low temperatures, up to 500 °C: $Zn_3(PO_4)_2 \cdot 2H_2O \rightarrow \alpha$-$Zn_3(PO_4)_2 \rightarrow \gamma$-$Zn_3(PO_4)_2$, and the α phase derived from hopeite is transformed to the β phase rather than the γ phase.

Electrochemical corrosion tests were performed to investigate how the various conversion phases affect the ability of the crystal coatings to protect the steel from corrosion. This protective ability was estimated by making comparisons between the corrosion potential, E_{corr}, values obtained from the potential axis at the transition point from the cathodic to anodic sites on the electrochemical polarization curves. As summarized in Table I, no appreciable changes in the E_{corr}

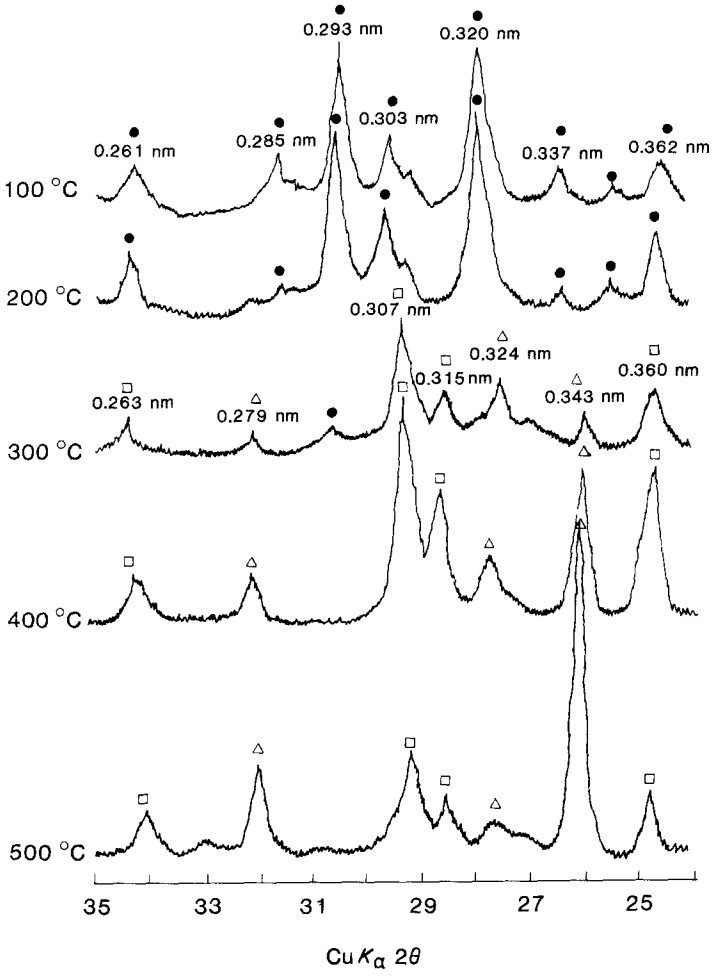

Figure 3 XRD patterns of 100°, 200°, 300°, 400° and 500 °C treated Zn·Ph layers; $Zn_3(PO_4)_2 \cdot 2H_2O$ (●), α-$Zn_3(PO_4)_2$ (□) and γ-$Zn_3(PO_4)_2$ (△).

TABLE I Phase changes in conversion coating with E_{corr}

Temperature (°C)	Phase		E_{corr}[a] (V)
	Major	Minor	
100	$Zn_3(PO_4)_2 \cdot 2H_2O$	—	− 0.573
200	$Zn_3(PO_4)_2 \cdot 2H_2O$	—	− 0.572
300	α-$Zn_3(PO_4)_2$	γ-$Zn_3(PO_4)_2$	− 0.572
400	α- and γ-$Zn_3(PO_4)_2$	—	− 0.600
500	γ-$Zn_3(PO_4)_2$	α-$Zn_3(PO_4)_2$	− 0.657

[a] In aerated 0.5 M NaCl solution.

values for samples treated at temperatures up to 300 °C were observed. A shift in E_{corr} to a more negative site occurred when the samples were baked at 400 °C, thereby indicating that the hybrid layers of α-$Zn_3(PO_4)_2$ and γ-$Zn_3(PO_4)_2$ have less corrosion resistance. A further increase in the treatment temperature to 500 °C resulted in a significant reduction in E_{corr}. Thus, it was found that the corrosion-protective ability of the Zn·Ph layers is dependent upon the extent of the conversion from the α phase to the γ phase, but independent of the dehydration and elimination of crystallized water in the Zn·Ph layers which occurs at a temperature of approximately 300 °C in air. The possible reason for the poor protective behaviour of the Zn·Ph layers containing the γ phase is the increased porosity of the crystal layers. This can be seen in the SEM images shown in Fig. 4. Namely, the SEM micrograph at the bottom of the figure which is of a 500 °C-treated sample surface indicates the presence of numerous microcracks on the crystal faces. Fig. 4 also gives the results of elemental intensity count ratios for iron or phosphorus to zinc atoms obtained by EDX quantitative analyses. These results show that the P–Zn ratio decreases with increased temperature and that no significant changes occur in the Fe–Zn ratio at temperatures up to 500 °C. This implies that some of the phosphorus atoms are eliminated as a result of heating in air.

Fig. 5 shows SEM micrographs and accompanying EDX elemental analyses for the heat-treated samples after exposure to a 0.1 M NaOH solution for 1 h. From the viewpoint of surface topographics, the SEM image for the exposed 100 °C-samples reveals a random distribution of roundish microcrystals. The alteration to a roundish shape from the original angular shape appears to be due to dissolution of the crystal caused by the attack of the NaOH solution. In connection with this, the EDX P–Zn ratio was reduced significantly from that of the corresponding unexposed sample (see Fig. 4 – 100 °C). It is clear that a large amount of phosphate was removed by the alkaline dissolution of the Zn·Ph crystals. In contrast, the Fe–Zn ratio changed very little.

The extent of the alkaline dissolution of the Zn·Ph can be estimated from the amount of reduction in the P–Zn ratios as determined by comparisons of the EDX quantitative data for samples before and after exposure. Attention was, therefore, given to the changes in the P–Zn ratio of the samples as a function of temperature. The resulting EDX data indicate that

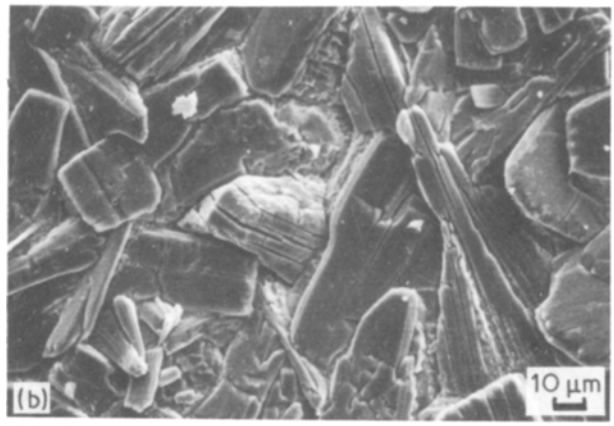

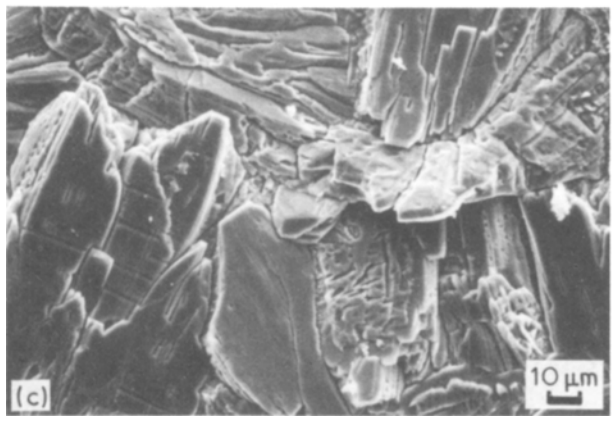

Figure 4 SEM photographs (a) 100°, (b) 300° and (c) 500 °C treated Zn·Ph surfaces.

Element	Before exposure intensity ratio/Zn		
	100 °C	300 °C	500 °C
Iron	0.85	0.79	0.80
Zinc	1.00	1.00	1.00
Phosphorus	0.96	0.86	0.81

the P–Zn ratios for the exposed samples were lower than for unexposed ones, and the magnitude depends primarily on the treatment temperature; namely, the reduction rate conspicuously decreases with an

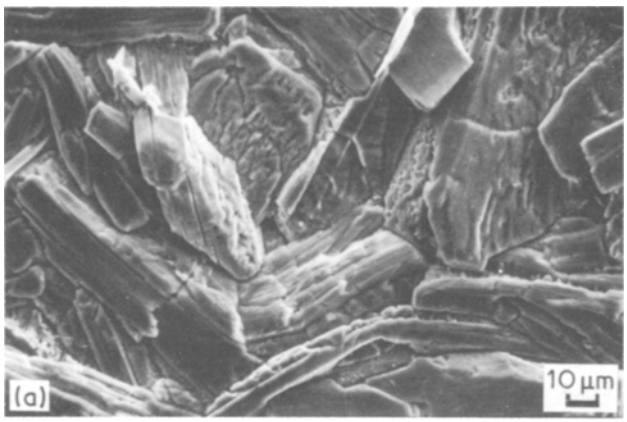

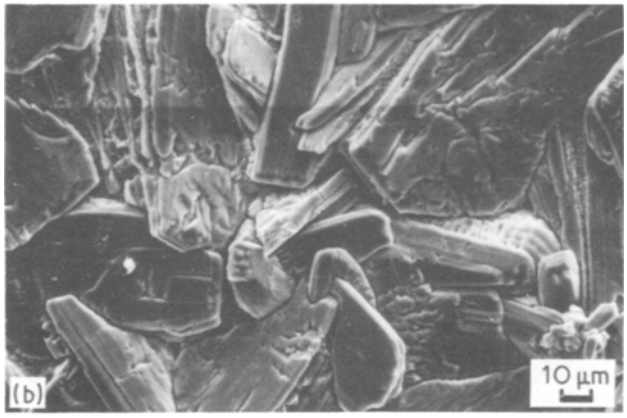

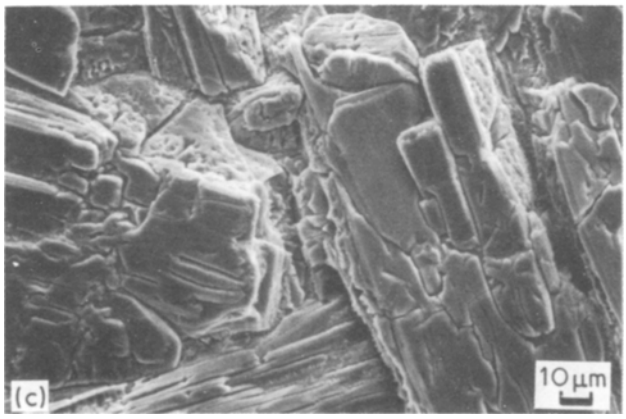

Figure 5 SEM images and EXD data for thermally treated Zn·Ph surfaces after exposure to 0.1 M NaOH for 1 hr. (a) 100 °C, (b) 300 °C, (c) 500 °C.

Element	After exposure to NaOH intensity ratio/Zn		
	100 °C	300 °C	500 °C
Iron	0.81	0.62	0.84
Zinc	1.00	1.00	1.00
Phosphorus	0.45	0.72	0.82

increase in treatment temperature. However, at 500 °C, the P–Zn ratios for samples before and after exposure were essentially the same, thereby suggesting that γ phase-rich crystal layers are less susceptible to alkaline dissolution. Thus, the magnitude of alkaline dissolution for the Zn·Ph compounds seems to be in the order of $Zn_3(PO_4)_2 \cdot 2H_2O > \alpha\text{-}Zn_3(PO_4)_2 > \gamma\text{-}Zn_3(PO_4)_2$.

Polarization curves for 100, 300 and 500 °C treated samples after exposure to a 0.1 M NaOH solution for 1 h are given in Fig. 6. The shape of the curves represents the transition from cathodic polarization at the onset of the most negative potential to the anodic polarization curves at the end of the lower negative potential. The potential axis at the transition point from cathodic to anodic curves is normalized as the corrosion potential, E_{corr}. These polarization behaviours were determined in an aerated 0.5 M NaCl solution at 25 °C. Comparisons of the cathodic polarization areas for the 300 and 500 °C treated samples with that for the 100 °C treated sample indicated the following: (1) at 500 °C, the short-term steady-state current value in the potential region between − 1.0 and − 1.1 V is considerably higher, (2) heat treatment at 300 °C shifts the E_{corr} to a more positive site and decreases the current density at the potential axis, and (3) treatment at 500 °C decreases E_{corr} and enhances the current density in the vicinity of E_{corr}. Although the 500 °C treated Zn·Ph is less susceptible to alkaline dissolution, the higher current density (observation (1) above) is indicative of high oxygen reduction kinetics which occur under the coating. The reason for this enhanced oxygen reduction reaction, $H_2O + \frac{1}{2}O_2 + 2e^- = 2OH^-$, in an aerated NaCl solution may be due to the increased porosity of the coating caused by the $\alpha \rightarrow \gamma$ phase transitions during heating at 500 °C, thereby resulting in a poor protective performance. In addition, a coating exhibiting a poor protective nature would be expected to display a lower E_{corr} and a higher current density. This is in agreement with observation (3). With regards to observation (2), the conversion to an anhydrous α phase at 300 °C yields a more stable layer and inhibits the oxygen reduction reaction. It appears that this relates directly with the low-rate of alkaline dissolution.

4. Conclusions

The water of crystallization in the $Zn_3(PO_4)_2 \cdot 2H_2O$ major phase of Zn·Ph conversion coatings deposited on steel surfaces through dissolution–recrystallization processes using zinc orthophosphate dihydrate powders is eliminated by heating in air at temperature between 300 and 400 °C. The kinetics for the thermal dehydration of the hydrous crystal coatings are related directly to the following phase transition at temperatures up to 500 °C;

$$Zn_3(PO_4)_2 \cdot 2H_2O \xrightarrow{300\,^\circ C} \alpha\text{-}Zn_3(PO_4)_2 \gg$$

$$\gamma\text{-}Zn_3(PO_4)_2 \xrightarrow{400\,^\circ C} \alpha\text{-}Zn_3(PO_4)_2$$

and

$$\gamma\text{-}Zn_3(PO_4)_2 \xrightarrow{500\,^\circ C} \gamma\text{-}Zn_3(PO_4)_2 \gg \alpha\text{-}Zn_3(PO_4)_2$$

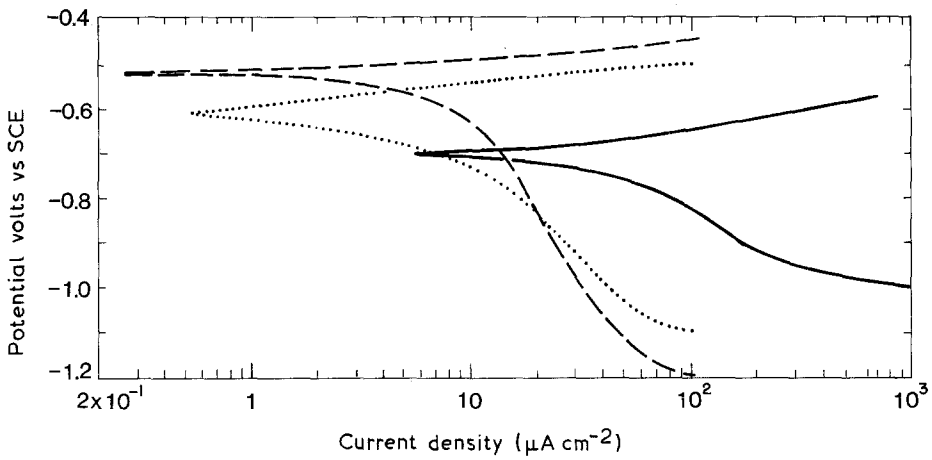

Figure 6 Polarization curves for 100 °C (····) 300 °C (– – –) 500 °C (——) treated zinc phosphated steels after immersion in 0.1 M NaOH.

When the corrosion-protective ability of these conversion phases was studied, it was determined that anhydrous α phase-rich crystal layers yielded at 300 °C had the same protective ability as hydrous conversion coatings. Heat treatment at 500 °C as a means of producing γ phase-rich coatings, however, led to a poor protective behaviour. This was due to an increase in the number of microcracks on the crystal faces caused by α → γ phase transition. This suggests that the corrosion-protective ability of Zn·Ph layers at high temperatures is dependent on the extent of the conversion from α to γ phases, but independent of the dehydration and elimination of crystallized water in the Zn·Ph layers.

The anhydrous α and γ phases were also found to be less susceptible to alkaline dissolution of Zn·Ph crystals, thereby resulting in a lower rate of phosphorus dissociation from the crystal layers. The microcrack-free α phase layers at 300 °C yielded the best protection performance for the crystal-covered steel systems upon exposure to a NaOH solution.

Acknowledgements

This work was performed under the auspices of the US Department of Energy, Washington, DC under contract DE-ACO2-76CH00016 and supported by the US Army Research Office Program MIPR-ARO-103-88.

References

1. T. SUGAMA, L. E. KUKACKA, N. CARCIELLO and J. B. WARREN, *J. Coatings Tech.* **61** (1989) 43.
2. T. SUGAMA, L. E. KUKACKA, N. CARCIELLO and J. B. WARREN, *J. Mater. Sci.* **19** (1984) 4045.
3. C. E. SROOG, *J. Polym. Sci., Macromol Rev.* **11** (1976) 161.
4. H. VOGEL and C. S. MARVEL, *J. Polym. Sci.* **50** (1961) 511.
5. J. K. STILLE and J. R. WILLIAMS, *ibid.* **B2** (1964) 209.
6. R. W. LENZ, *et al., ibid.* **50** (1962) 351.
7. R. KOJIMA, H. OKITA and Y. MATSUSHIMA, *Tetsu to Hagane* **66** (1980) 924 (Japanese).
8. A. J. SOMMER and H. L. LEIDHEISER, Jr., *Corrosion* **43** (1987) 661.

Received 9 December 1988
and accepted 31 May 1989